Journal of Sound and Vibration 421 (2018) 61–78

Contents lists available at ScienceDirect

Journal of Sound and Vibration

journal homepage: www.elsevier.com/locate/jsvi

Comparative methods to assess harmonic response of nonlinear piezoelectric energy harvesters interfaced with AC and DC circuits

Chunbo Lan [a, c], Lihua Tang [a, *], Ryan L. Harne [b]

[a] Department of Mechanical Engineering, University of Auckland, Auckland, 1010, New Zealand
[b] Department of Mechanical and Aerospace Engineering, The Ohio State University, Columbus, OH 43210, USA
[c] Department of Engineering Mechanics, Northwestern Polytechnical University, Xi'an, 710072, People's Republic of China

ARTICLE INFO

Article history:
Received 27 August 2017
Received in revised form 8 November 2017
Accepted 11 November 2017

Keywords:
Nonlinear energy harvesting
Piezoelectric
Monostable
AC and DC interface circuits

ABSTRACT

Nonlinear piezoelectric energy harvester (PEH) has been widely investigated during the past few years. Among the majority of these researches, a pure resistive load is used to evaluate power output. To power conventional electronics in practical application, the alternating current (AC) generated by nonlinear PEH needs to be transformed into a direct current (DC) and rectifying circuits are required to interface the device and electronic load. This paper aims at exploring the critical influences of AC and DC interface circuits on nonlinear PEH. As a representative nonlinear PEH, we fabricate and evaluate a monostable PEH in terms of generated power and useful operating bandwidth when it is connected to AC and DC interface circuits. Firstly, the harmonic balance analysis and equivalent circuit representation method are utilized to tackle the modeling of nonlinear energy harvesters connected to AC and DC interface circuits. The performances of the monostable PEH connected to these interface circuits are then analyzed and compared, focusing on the influences of the varying load, excitation and electromechanical coupling strength on the nonlinear dynamics, bandwidth and harvested power. Subsequently, the behaviors of the monostable PEH with AC and DC interface circuits are verified by experiment. Results indicate that both AC and DC interface circuits have a peculiar influence on the power peak shifting and operational bandwidth of the monostable PEH, which is quite different from that on the linear PEH.

1. Introduction

Recently, researchers have been searching alternatives to harvest vibration energy in environment to provide a green power supply for small devices. To enlarge the operational bandwidth and improve the output power, nonlinear dynamics [1–4] have been widely introduced in the piezoelectric energy harvesters (PEH). Nonlinear systems such as Duffing-type PEH have been widely investigated and shown significant improvements in bandwidth and harvested power [5–8]. The main superiority of these nonlinear PEHs as compared to the linear PEH is the existence of high-energy oscillations in a wide frequency bandwidth [9]. When the nonlinear PEH surfs on the high-energy orbits, a huge output power enhancement can be

* Corresponding author.
E-mail address: l.tang@auckland.ac.nz (L. Tang).

https://doi.org/10.1016/j.jsv.2017.11.019
0022-460X/

achieved. Similar to these single degree of freedom (SDOF) nonlinear PEHs, the multi-DOF systems were added with the magnetic interaction induced nonlinearity to pursue a wide operational bandwidth recently. Two kinds of 2-DOF nonlinear PEHs have obtained preliminary results [10–15]. One is using the magnetic force to integrate two independent SDOF systems (such as cantilever piezoelectric beams), while the other is adding the magnets forces into a linear 2DOF PEH. Both configurations can be further designed into monostable [10], bistable [11,12] and even multistable. Results of the first configuration show that high-energy oscillations around the first and second resonances maintain a much wider operational bandwidth than that in SDOF nonlinear PEHs. Meanwhile, internal resonance and modal interactions [13,14,16,17] clearly observed in the second configurations have attracted great interests due to an energetic saturation vibration and enhanced energy transfer between modes that promote an exceptional wide-bandwidth harvesting performance.

Along with the abundant designs of nonlinear PEHs, the electric circuits for energy conversion and storage also received great attentions. In application, the alternating current generated by piezoelectric patches needs to be transformed into direct currents. Indeed, standard rectifying circuits (DC interface) are required to interface the PEH and electronic load in practice. Researchers have designed advanced nonlinear circuits, such as resistive impedance matching circuit [18] and parallel/series-SSHI (synchronized switch harvesting on inductor) [19,20], to improve the efficiency of energy harvesting. Hence, it is of great importance to understand the inherent relations between circuits and the dynamics of linear/nonlinear piezoelectric energy harvesters. Shu and Lien [21] investigated the optimal AC-DC power generation for a linear piezoelectric PEH. The trends in vibration, rectified voltage and average power observed in Ref. [25] are indeed very similar to those of AC circuit in Ref. [22]. As the resistance increases, there are two power peaks, one is close to the open circuit while the other is close to the short circuit when the electromechanical coupling coefficient is strong enough. Rupp et al. [23] developed a computational methodology based on harmonic balance method for accurate analysis of the interaction between linear piezoelectric PEHs and a nonlinear circuit with diodes. As the inherent relations between linear PEHs and standard rectifying circuits becoming clear, a few researches begin to explore the role of non-rectifying and rectifying circuits on the nonlinear PEHs. Liu et al. [24] evaluated a bistable PEH connected to DC and SSHI circuits and observed unique impacts from such advanced circuits upon the power generation outputs as compared to that by connecting an AC interface circuit. Yet, the comprehensive understanding of the influences of these rectifying circuits on the behaviours of nonlinear piezoelectric energy harvesters are still inadequate. Given the sensitivities of nonlinear PEH observed in the studies surveyed above, such as ability or inability to induce the high-energy oscillations, it is critical to identify the roles of the realistic rectifying circuits upon the dynamics of nonlinear PEHs.

Given these unknowns, a preliminary research focusing on the effect of load resistance on the dynamics of monostable PEH has been conducted by authors in Ref. [25]. It is observed in the simulations that the increase of resistance will result in an exceptional shift of power peak. In this work, we are motivated to further explore the effect of AC and DC interfaces circuits on the nonlinear dynamics of monostable PEH in a more generic scenario (various load resistances, excitations, electromechanical coupling strengths) and more importantly, ascertain the inherent mechanisms behind these interesting phenomena. First, we conduct harmonic balance analysis and equivalent circuit modeling (ECM) to predict performances of nonlinear PEH with AC and DC interface circuits. By using these methods, we are interested to figure out how the two circuits affect the nonlinear dynamics and how it in turn affects the performance of monostable PEH. The theoretical and simulation results are experimentally validated and reveal the similarities and differences in the trend of the resonant power peak shift against various load resistances in AC and DC interfaces and the sensitivity to excitation. Further analysis and simulation also unlock the influence of electromechanical coupling strength on the power output for both interface circuits.

2. Modeling

The schematic of the nonlinear piezoelectric energy harvester investigated in this paper is shown in Fig. 1. It is made of a piezoelectric bimorph cantilever with a tip mass. The tip mass carries a permanent magnet that interacts with another magnet held in the acrylic holder attached to the rig. The threaded acrylic holder is movable, thus the repulsive magnetic force between these two magnets can be adjusted by tuning the distance between the magnets. When the magnetic force is large enough to make the cantilever beam buckle, the system turns to be a bistable PEH. Otherwise, it is a monostable or quasi-linear PEH. The governing equations of this kind of nonlinear PEH can be written according to the fundamental, lowest-order mode of dynamic response using

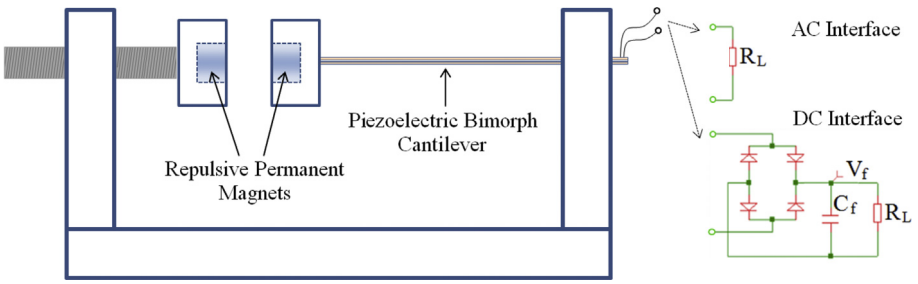

Fig. 1. Schematic of monostable PEH connected to AC or DC interface circuit.

$$M_{\text{eff}}\ddot{x}(t) + C_{\text{eff}}\dot{x}(t) + K_{\text{eff}}x(t) - \Theta V(t) + F_{\text{magnet}} = -M_{\text{eff}}\ddot{y}(t) \tag{1}$$

$$I(t) + C_{\text{p}}\dot{V}(t) + \Theta\dot{x}(t) = 0 \tag{2}$$

where M_{eff}, C_{eff} and K_{eff} are the effective mass, damping and stiffness respectively. For the cantilever beam of monostable configuration, the effective mass and stiffness can take the following forms [26] $M_{\text{eff}} = \beta_M A_b L\rho + Mt$, $K_{eff} = (\beta_K EI)/L^3$, where ρA_b and EI are the mass per unit length and bending stiffness of the cantilever beam, respectively, and L is the length of cantilever beam. β_M and β_K are coefficients related to the dynamic mode shape and strain distribution of the cantilever beam, and they can be determined based on the energy conservation principle. The effective damping is then obtained by $C_{\text{eff}} = 2\zeta\omega_{\text{n}}M_{\text{eff}}$, where ζ is the damping ratio determined by utilizing the logarithmic decrement method in experimental test; Θ is the electromechanical coupling coefficient; C_{p} is the clamped capacitance of the piezoelectric transducer; $y(t) = Y\sin(\omega t))$ and $x(t)$ are the displacement of the base and the displacement of the tip mass relative to the base, respectively; $V(t)$ is the voltage across the piezoelectric transducer; $I(t)$ is the current flowing into the interface circuit; and F_{magnet} is the magnetic force.

This model includes nonlinear restoring force (from magnets), but assumes a linear electromechanical coupling behaviour. The dipole-dipole magnetic interaction model [27] is frequently used in the literature to describe the repulsive force and potential energy between two magnets. The potential energy between two magnets is

$$U(x) = \frac{\tau m_1 m_2}{2\pi}\left(x^2 + D^2\right)^{-\frac{3}{2}} \tag{3}$$

where $\tau = 4\pi \times 10^{-7}$ NA^{-2} is the permeability constant in vacuum; m_1 and m_2 are the effective magnetic moments of the magnetic dipoles. In this study, $m_1 = m_2 = m = 0.164$ Am^2. D is the center-to-center distance between two magnets. Hence, $D = D_0 + \Delta$, where D_0 is the surface-to-surface distance between magnets and $\Delta = 3$ mm is the thickness of magnet. The magnetic force can be derived by differentiating Eq. (3) with respect to x,

$$F_{\text{magnet}}(x) = f_0\frac{x}{\left(x^2 + D^2\right)^{\frac{5}{2}}} \tag{4}$$

where $f_0 = -3\tau m^2/(2\pi)$. For the convenience of harmonic balance analysis in the next sections, Eq. (4) is expanded in a Taylor series about $x = 0$. By ignoring series terms of order greater than 3, we obtain

$$F_{\text{magnet}}(x) = K_1 x + K_3 x^3 \tag{5}$$

where $K_1 = f_0 D^{-5}, K_3 = -2.5 f_0 D^{-7}$.

Moreover, $V(t)$ and $I(t)$ are related in different ways according to the interface circuit property. When a PEH is connected to a pure resistor R_{L}, the relation between the voltage and current is linear with $V(t) = I(t)\,R_{\text{L}}$. Thus, Eq. (2) can be rewritten as

$$\frac{V(t)}{R_{\text{L}}} + C_{\text{p}}\dot{V}(t) + \Theta\dot{x}(t) = 0 \tag{6}$$

When the PEH is connected to a standard rectifying DC interface circuit, the current balance equations can be derived based on the Schockley model by Leadenham [28]. They are

$$C_{\text{p}}\dot{V}(t) + \Theta\dot{x}(t) + 2I_{\text{s}}\sinh\left(\frac{V(t)}{2nV_{\text{T}}}\right)\exp\left(\frac{-V_{\text{f}}(t)}{2nV_{\text{T}}}\right) = 0 \tag{7}$$

$$C_{\text{f}}\dot{V}_{\text{f}}(t) + V_{\text{f}}(t)/R_{\text{L}} + 2I_{\text{s}}\left[1 - \cosh\left(\frac{V(t)}{2nV_{\text{T}}}\right)\exp\left(\frac{-V_{\text{f}}(t)}{2nV_{\text{T}}}\right)\right] = 0 \tag{8}$$

where C_{f} is the capacitance of the filter capacitor; $V_{\text{f}}(t)$ is the output voltage across the filter capacitor (same voltage across the load resistor); $I_{\text{s}} = 1$ pA is the saturation current of diode, which is a constant; $n = 1$ is the ideality factor of diode; the thermal voltage defined as $V_{\text{T}} = 26$ mV at room temperature. Thus, Eqs. (1), (7) and (8) constitute the governing equations of the monostable PEH with DC interface circuit.

2.1. Harmonic balance analysis

2.1.1. Monostable PEH with AC interface

When the dynamics of nonlinear energy harvesters connected to an AC interface circuit are considered, a variety of approximate analytical methods, such as harmonic balance method [29] or method of multiple scales [30], may directly

predict the power generation for a given nonlinear harvester design and implementation. In this paper, harmonic balance method is chosen for theoretical analysis. It has been used in the literature when deriving the approximate steady state solutions for bistable PEH [29,31], tri-stable PEH [32], and so on. The detailed deviation of monostable PEH's steady solutions is similar to that of bistable PEH given in Ref. [29]. The frequency-amplitude response is obtained as,

$$r^2\left[\left(-\omega^2 M_{\text{eff}}+k_0+\frac{3}{4}r^2K_3+\frac{C_{\text{p}}(\Theta R_{\text{L}}\omega)^2}{(C_{\text{p}}R_{\text{L}}\omega)^2+1}\right)^2+\left(\omega C_{\text{eff}}+\frac{\Theta^2 R_{\text{L}}\omega}{(C_{\text{p}}R_{\text{L}}\omega)^2+1}\right)^2\right]=f^2 \tag{9}$$

where r is the displacement amplitude of the monostable PEH; $k_0=K_{\text{eff}}+K_1$; $f=M_{\text{eff}}A_0$ is the amplitude of the excitation force, where $A_0=Y\omega^2$ is the amplitude of the acceleration. The detailed derivation is shown in the Appendix. To determine the stability of the physically meaningful solutions obtained from Eq. (9), the method in Ref. [29] is applied.

Additionally, from the derivation, we find that the effect of AC interface circuit can be regarded as equivalent stiffness and damping,

$$K_{\text{AC}}=\frac{(R_{\text{L}}\omega\Theta)^2C_{\text{p}}}{(C_{\text{p}}R_{\text{L}}\omega)^2+1},c_{\text{AC}}=\frac{\Theta^2R_{\text{L}}}{(C_{\text{p}}R_{\text{L}}\omega)^2+1} \tag{10}$$

It is indicated that the equivalent stiffness K_{AC} and equivalent damping c_{AC} induced by the interface circuit depend on the external excitation frequency ω, the load resistance R_{L}, the capacitance of the piezoelectric element C_{p}, and the electromechanical coupling Θ. Interestingly, it is noted that the expressions of K_{AC} and c_{AC} are independent of the vibration systems, that is, the change of stiffness and damping are the same to linear and monostable PEHs.

2.1.2. Monostable PEH with DC interface

In the case of monostable PEH with DC interface circuit, a Newton's method enabled harmonic balance method is utilized to get the approximate solutions. This method has been successfully applied to identify the effect of piezoelectric material induced nonlinearity on the PEH with DC interface circuit [28]. The principle is shown below and derives from the theory described in Ref. [33].

First, it is necessary to describe the system in the state-space form as

$$\dot{\mathbf{u}}=\boldsymbol{f}(t,\mathbf{u}) \tag{11}$$

where $\mathbf{u}$ is the state vector and defined as

$$\mathbf{u}=[\,u_1\quad u_2\quad u_3\quad u_4\,]^{\mathbf{T}}=[\,x\quad\dot{x}\quad V\quad V_{\text{f}}\,]^{\mathbf{T}} \tag{12}$$

Hence, the governing Eqs. (1), (7) and (8) are rearranged into state-space form as

$$\begin{cases}\dot{u}_1=u_2\\ \dot{u}_2=-\ddot{y}(t)-\left(C_{\text{eff}}u_2+K_{\text{eff}}u_1-\Theta u_3+K_1u_1+K_3u_1^3\right)\Big/M_{\text{eff}}\\ \dot{u}_3=\left(-\Theta u_2-2I_{\text{s}}\sinh\left(\frac{u_3}{2nV_{\text{T}}}\right)\exp\left(\frac{-u_4}{2nV_{\text{T}}}\right)\right)\Big/C_{\text{p}}\\ \dot{u}_4=\left(-\frac{u_4}{R_{\text{L}}}-2I_{\text{s}}\left[1-\cosh\left(\frac{u_3}{2nV_{\text{T}}}\right)\exp\left(\frac{-u_4}{2nV_{\text{T}}}\right)\right]\right)\Big/C_{\text{f}}\end{cases} \tag{13}$$

By assuming that Eq. (11) has periodic solutions with period T, the approximate solutions are expressed in term of Fourier series as

$$\mathbf{u}(t)=\mathbf{u}(t+T,\mathbf{u}) \tag{14}$$

$$\widehat{\mathbf{u}}(t)=\mathbf{a}+\mathbf{A}\mathbf{c}(t)+\mathbf{B}\mathbf{s}(t) \tag{15}$$

where $\mathbf{a}$ is a constant vector, $\mathbf{A}$ and $\mathbf{B}$ are constant matrices, and $\mathbf{c}(t)$ and $\mathbf{s}(t)$ are vectors of cosines and sines of harmonics. The component form is

$$\widehat{u}_i(t)=a_i+\sum_{m=1}^{M}[A_{im}c_m(t)+B_{im}s_m(t)] \tag{16}$$

with indices,

$m, n \in [1, 2, \ldots, M]$,

$$c_m(t) = \cos\left(\frac{2\pi mt}{T}\right), s_m(t) = \sin\left(\frac{2\pi mt}{T}\right)$$

where M is the number of harmonics included in the truncated Fourier series solution. The derivative of $\mathbf{u}(t)$ can be written as

$$\dot{\hat{u}}_i(t) = \frac{2\pi m}{T}\sum_{m=1}^{M}[-A_{im}s_m(t) + B_{im}c_m(t)] \tag{17}$$

Substituting the assumed solution $\hat{u}_i(t)$ into the governing equations $\mathbf{f}(t,\mathbf{u})$, yields the approximate system,

$$\hat{\mathbf{f}}(t) = \mathbf{f}(t, \hat{\mathbf{u}}(t)\Big) \tag{18}$$

The residual is defined as

$$\mathbf{r}(t) = \hat{\mathbf{f}}(t) - \dot{\hat{\mathbf{u}}}(t) \tag{19}$$

By utilizing Galerkin method to minimizing the residual, we obtain

$$\frac{1}{T}\int_0^T \mathbf{r}(t)dt = 0;\ \frac{1}{T}\int_0^T \mathbf{r}(t)\mathbf{c}^T(t)dt = 0; \frac{1}{T}\int_0^T \mathbf{r}(t)\mathbf{s}^T(t)dt = 0 \tag{20}$$

Eq. (20) is a system of $2M + 1$ unknowns that can be solved for the correct **a**, **A** and **B**. Hence the approximate solutions are obtained.

The error minimization procedure steps towards a defined error tolerance by the way of approximating the derivatives of the residual and updating a subsequent step with a refined initial guess. The derivative approximation approach used in this research is described in Refs. [28,33].

To seed the initial guess to the model, an effective method must be employed due to the non-uniqueness of dynamic states possible for the monostable PEH. Here, the closed-form analytical results obtained from a harmonic balance analysis of the monostable PEH coupled to an AC interface circuit are first computed [34]. This analysis requires on the order of milliseconds to compute across the full frequency range of interest. The outputs of such analysis are the mechanical response and AC piezoelectric voltage response constants. From these data, the corresponding **a**, **A**, and **B** constants are taken to be initial guesses of the mechanical response and piezoelectric voltage response for the monostable PEH interfaced to the DC interface circuit. In all cases, due to the monostability of the PEH, the constants **a** are nill. For the initial guess of the DC rectified voltage, the constants in **A** and **B** are nill. On the other hand, the DC voltage term, by definition, has a bias constant **a** to be initialized. Here, the square root of the sum of squares of the sinusoidal AC piezoelectric voltage constants from the analytical evaluation is taken, and the result is multiplied by $1/\sqrt{2}$. This value is consequently the corresponding constant **a** for the initial guess of the DC voltage term. For the DC interface circuit, stability is inherent to the output since an analytically derived Jacobian is provided to the algorithm. The results consequently converge to stable sets of the response variables [28,33].

2.2. Equivalent circuit model

By representing the monostable energy harvester as an equivalent circuit, the performance of the energy harvesting system with AC, DC, and even more advanced interface circuits (such as SSHI and SCE) can be evaluated with the help of mature SPICE electronics simulator (SIMetrix/SIMPLIS Introduction Version is used in this work). This idea has been proved feasible in the modeling of galloping based aeroelastic energy harvesting with various practical interface circuits, in which, the aerodynamics force is a nonlinear damping force [35,36]. This idea can be extended to study the PEH with structural nonlinearity subject to base excitation [14,25]. This simulation method will be utilized in the paper to conduct a comprehensive parametric study and confirm the findings from the theoretical analysis.

According to the analogies between the electrical and mechanical domains, the charge q, inductance L, capacitance C, resistance R, turn ratio of the ideal transformer N and voltage source V_S are equivalent to displacement x, mass M_{eff}, compliance $1/K_{\text{eff}}$, damping C_{eff}, electromechanical coupling coefficient Θ and force F, respectively. In the following experiment and simulation, sinusoidal sweep with constant magnitude of acceleration is considered as the input base excitation. The voltage source component representing the base motion is implemented by a linear chirp signal with magnitude of $M_{\text{eff}}A_0$. The nonlinear magnetic force F_{magnet} is implemented by a user defined behavioral voltage source, which can be defined using the voltage across capacitance C as input [14,25],

$$V_{S\_NL} = K_1 CV_C + K_3 (CV_C)^3 \tag{21}$$

The details in the implementation of a nonlinear behavioral voltage source can be found in Ref. [25].

3. Theoretical and simulation results

This section presents and compares the performances of the monostable PEH with AC and DC interface circuits. Three main factors affecting the power output and dynamics are studied: load resistance, acceleration and electromechanical coupling strength. The theoretical results are solved by using harmonic balance methods, while the simulation is carried out by equivalent circuit simulation. The preliminary study on the effect of resistance through equivalent circuit simulation and experiment was presented in our conference paper [25] and a small portion of the results is reused for comparison with theoretical analysis. In the simulation, the sine frequency sweep is carried out to obtain the frequency-response curves of the nonlinear energy harvester. Throughout the sine sweep, the peak acceleration is controlled at a constant value and the sweep rate in frequency is 0.02 Hz/s. The system parameters used in theoretical analysis and simulation are obtained from experimental tests, as listed in Table 1. The magnet distance $D_0 = 8.2$ mm is adjusted to obtain a typical monostable configuration.

3.1. AC interface

3.1.1. Effect of load resistance

The effect of load resistance on the monostable PEH with AC interface circuit is investigated in this section. The base acceleration amplitude is 2 ms^{-2}. Fig. 2(a) depicts the theoretical results of the output power against load resistance R_L. The unstable theoretical solutions are illustrated by dotted lines. Upward frequency sweep simulation is also performed and the simulation results are shown in Fig. 2(b). First, both simulation and theory show that the optimal resistance R_L is around 167 kΩ. Second, the resonant peak and bandwidth shift with the varying R_L is observed. Interestingly, the resonant peak shifts to the left and then returns to the right with the increase of R_L, with the turning point not exactly but very close to the optimal resistance $R_L = 167$ kΩ. These characteristics of the resonant peak shift of the monostable PEH observed in both theory and ECM simulation are different from its linear counterpart. In linear PEH, except for the strong electromechanical coupling, the optimal power will be achieved between the short circuit and open circuit resonant frequencies and the resonant peak will move all the way to the right with the increase of R_L. For the proposed prototype without magnetic force, the short circuit and open circuit resonant frequencies are measured to be 19.95 Hz and 20.25 Hz, respectively. Thus, the resonant peak of power will shift with R_L between these two frequencies. Obviously, given the same electromechanical coupling, the varying resistance has much more significant influence on the dynamics of monostable PEH than that on the linear PEH in terms of resonant peak shift and thus the associated bandwidth.

This phenomenon of resonant peak shift with the varying resistance can be explained from the view of equivalent stiffness and damping induced by AC interface circuit. The AC interface circuit induced equivalent stiffness K_{AC} and damping c_{AC} can be calculated by equation (10). The surfaces in Fig. 3(a) and (b) are the equivalent stiffness and damping respectively. The solid line with circles indicates the resonant peaks with various resistance and frequency. From Fig. 3, we note that with the increase of resistance, K_{AC} increases very slowly with R_L first, and then increases quickly, and finally reaches a maximum value (open circuit condition). While, c_{AC} starts to increase with R_L first, and then reaches the maximum and decreases (to zero eventually though not shown on Fig. 3(b)). In the open-circuit and short-circuit conditions, the AC circuit does not produce any equivalent damping to the system. The combination of these changes of K_{AC} and c_{AC} provides the trends of peak shift: when the resistance is very small, the effect of circuit-induced damping is predominant, which leads to the decrease of vibration, reduced nonlinear behaviour and thus the peak of power achieved at a lower frequency and a decrease of bandwidth. As the resistance increases and becomes large enough, the effect of circuit-induced stiffness becomes predominant. The power peak will shift to a higher frequency due to the increase of the total stiffness of the monostable PEH, though the circuit-induced damping may still increase. In this case, the main effect of circuit-induced damping is decreasing the magnitude of output power rather than frequency shift. Obviously, there is a trade-off between optimal power and operational bandwidth due to the combined effects of K_{AC} and c_{AC}. The resistance for the maximum power and wide operational bandwidth should compromise.

Table 1
Parameters obtained from experiment.

Parameters	Symbol	Value
Effective mass	M_{eff}	0.0082 kg
Effective stiffness	K_{eff}	138.6 Nm^{-1}
Damping ratio	ζ	0.016
Effective damping	C_{eff}	0.0354 Nsm^{-1}
Electromechanical coupling coefficient	Θ	599 μNV^{-1}
Capacitance of piezoelectric transducer	C_p	87 nF
Filter capacitance	C_f	4.7 μF

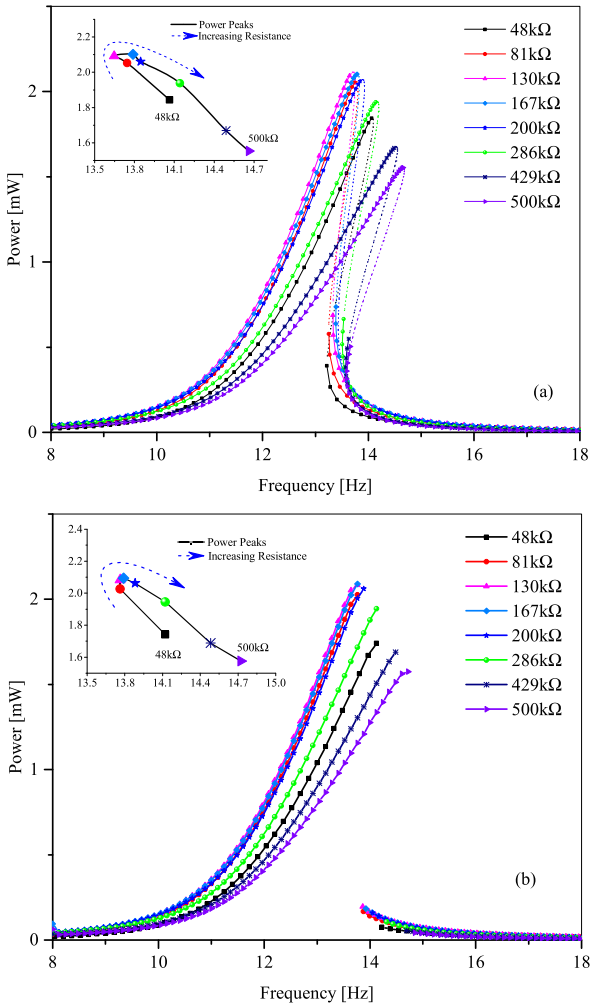

Fig. 2. Output powers of theory and ECM with AC interface circuit for weak electromechanical coupling ($\Theta = 599\ \mu N/V$, $A_0 = 2.0\ ms^{-2}$). (a) theory; (b) ECM [25].

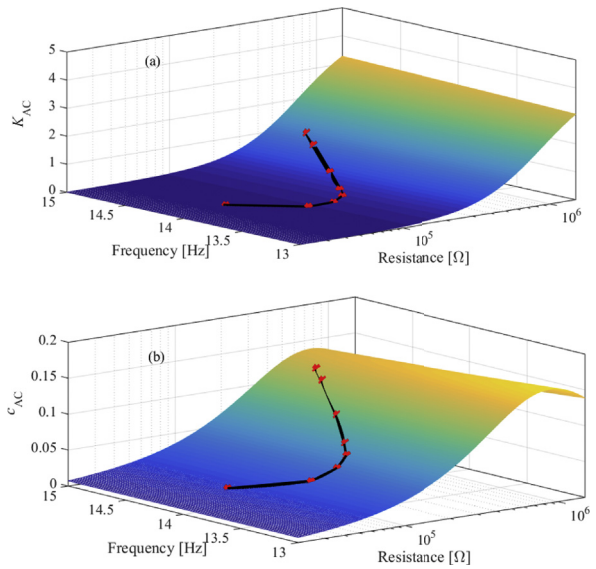

Fig. 3. (a) Equivalent stiffness K_{AC} and (b) equivalent damping c_{AC} induced by weak electromechanical coupling ($\Theta = 599\ \mu N/V$, $A_0 = 2.0\ ms^{-2}$).

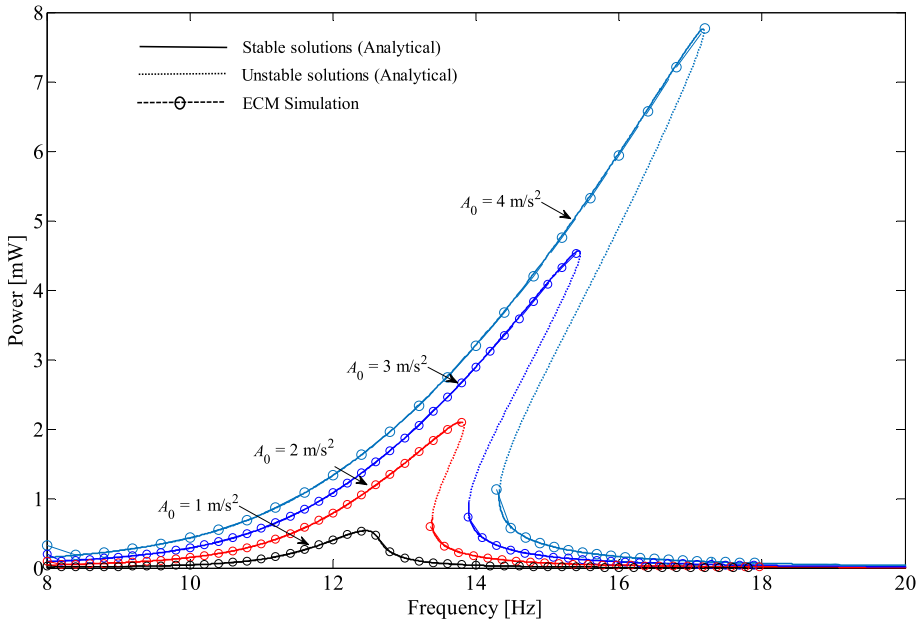

Fig. 4. Output powers of theory and ECM with AC interface circuit for different accelerations ($\Theta = 599$ μN/V, $R_L = 167$ kΩ).

3.1.2. Effect of excitation

Fig. 4 gives the output power of the monostable PEH under different accelerations. The resistance used in the analysis, $R_L = 167$ kΩ is the optimal resistance obtained from the previous section. The base accelerations are varied: $A_0 = 1$ ms^{-2}, 2 ms^{-2}, 3 ms^{-2}, 4 ms^{-2}. In Fig. 4, both theoretical and ECM simulation agree quite well, showing that the bandwidth and resonant peak will increase with the increase of excitation. Specifically, when the excitation is very low, such as $A_0 = 1$ ms^{-2}, there is no jumping phenomenon and no region with coexisting responses. As the acceleration increases, the region of coexisting responses becomes wider and the power peak increases accordingly. Hence, it is concluded that under strong excitation, the monostable PEH with AC interface possesses the capability of broadband energy harvesting.

3.1.3. Effect of electromechanical coupling strength

In section 3.1.1, the effect of resistance on the monostable PEH with a weak electromechanical coupling coefficient is analyzed. Since the coupling coefficient can largely affect the performance of AC interface circuit, a much strong coupling coefficient $\Theta = 2000$ μN/V is chosen in this section to make a comparative study. The acceleration is kept at $A_0 = 2$ ms^{-2} and the varying resistances are listed in Table 2.

Fig. 5(a) and (b) depict the theoretical prediction and ECM simulation (upward sweep) result of output powers of AC interface circuit against R_L, respectively. The unstable theoretical solutions are illustrated by dotted lines. First, both simulation and theoretical results show that there are two optimal resistances around 10 kΩ and 1500 kΩ. One is close to the short circuit condition and the other is close to the open circuit condition. Second, when the resistance R_L increases from 1 kΩ to 10 kΩ, the resonant peak of the monostable PEH shifts to the left and the region of coexisting responses becomes narrow gradually. It is noted that when R_L increases to 15 kΩ, the region of coexisting responses disappears (i.e., no jumping), while the resonance peak still keeps shifting to the left when R_L increases from 10 kΩ to 30 kΩ. Subsequently, when R_L continues to increase, the resonant peak turns to shift to the right and the power peak reaches the minimum value when $R_L = 130$ kΩ. After that, the increase of R_L leads to the increase of both resonant peak and frequency until R_L reaches the second optimal resistance around 1500 kΩ. Finally, when R_L further increases and exceeds 1500 kΩ, the resonant peak starts to decrease but keeps shifting to the right. Interestingly, it is found that the region of coexisting responses (jumping phenomenon) returns when R_L goes beyond 2500 kΩ.

To explain this evolution, the equivalent damping c_{AC} and stiffness K_{AC} with this strong electromechanical coupling coefficient are calculated and shown in Fig. 6. The surfaces in Fig. 6(a) and (b) stand for the K_{AC} and c_{AC} respectively. The dashed curves with circles represent the resonance peaks at different frequencies and resistances. It is found that, when R_L increases from 1 kΩ to about 500 kΩ, the equivalent damping and stiffness increase. c_{AC} increases sharply while K_{AC} increases very gently. With the further increase of resistance, c_{AC} starts to decrease while K_{AC} keeps increasing. When the resistance is close to open circuit, the circuit-induced equivalent damping is close to zero and the circuit-induced equivalent stiffness reaches saturation. As a result, when R_L is small and close to short-circuit, the increase of resistance mainly leads to the resonant peak shift to lower frequency due to the sharply increased damping, reduced vibrating response and less nonlinear behaviour. After the jumping phenomenon disappears, the increase of c_{AC} mainly reduces the power of resonant peak. Although the increase

Table 2
Power peaks with strong electromechanical coupling for various resistances of AC interface.

Resistance (kΩ)	1	3	5	7	10	15	20	30
Peak Freq. (Hz)	14.96	14.21	13.69	13.32	12.95	12.58	12.36	12.21
Power (mW)	0.801	1.652	2.012	2.154	2.187	2.057	1.882	1.579
Resistance (kΩ)	48	81	130	167	200	286	429	500
Peak Freq. (Hz)	12.36	13.47	14.51	15.18	15.55	16.00	16.30	16.37
Power (mW)	1.236	0.949	0.944	1.012	1.091	1.310	1.617	1.737
Resistance (kΩ)	600	800	1000	1500	2000	2500		
Peak Freq. (Hz)	16.52	16.67	16.82	17.04	17.26	17.41		
Power (mW)	1.874	2.058	2.153	2.184	2.086	1.951		

of resistance also leads to an increase of K_{AC}, it increases gently and less dominant when R_L is close to the short-circuit condition. When the resistance exceeds 130 kΩ, the equivalent stiffness starts to essentially influence the dynamics of monostable PEH. The resonant peak turns to shift to the right due to the increase of total stiffness. The jumping phenomenon and nonlinear behaviour become evident again when $R_L = 2500$ kΩ, which is mainly due to the reduced circuit-induced damping (close to open-circuit condition) and enhanced vibrating response.

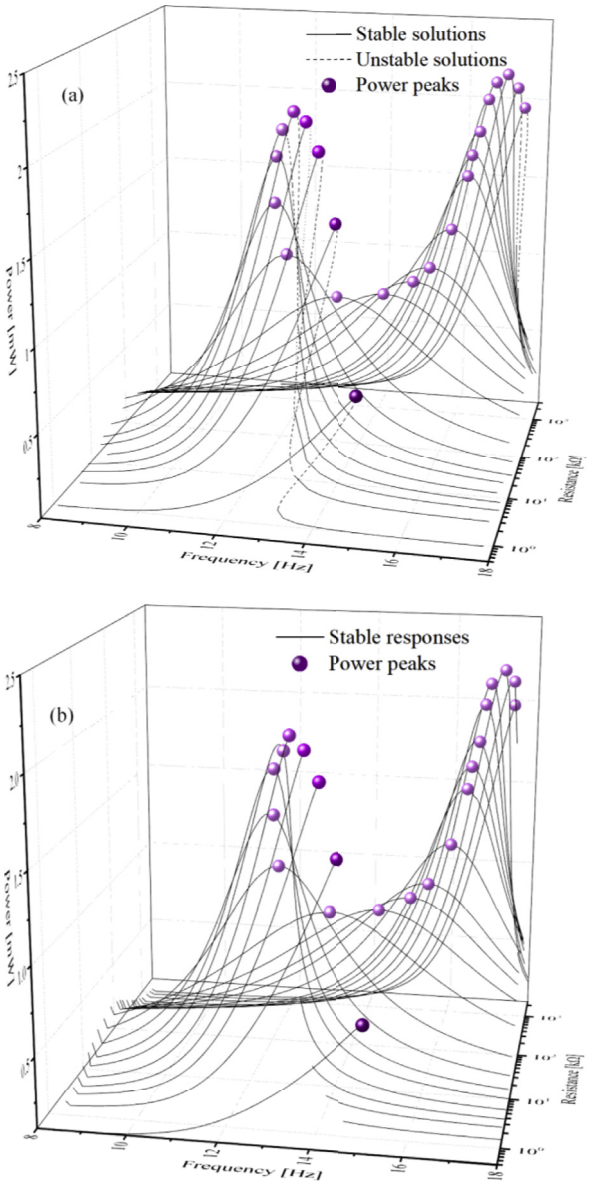

Fig. 5. Output powers of theory and ECM with AC interface circuit for strong electromechanical coupling ($\Theta = 2000$ μN/V, $A_0 = 2.0$ ms^{-2}). (a) theory; (b) ECM.

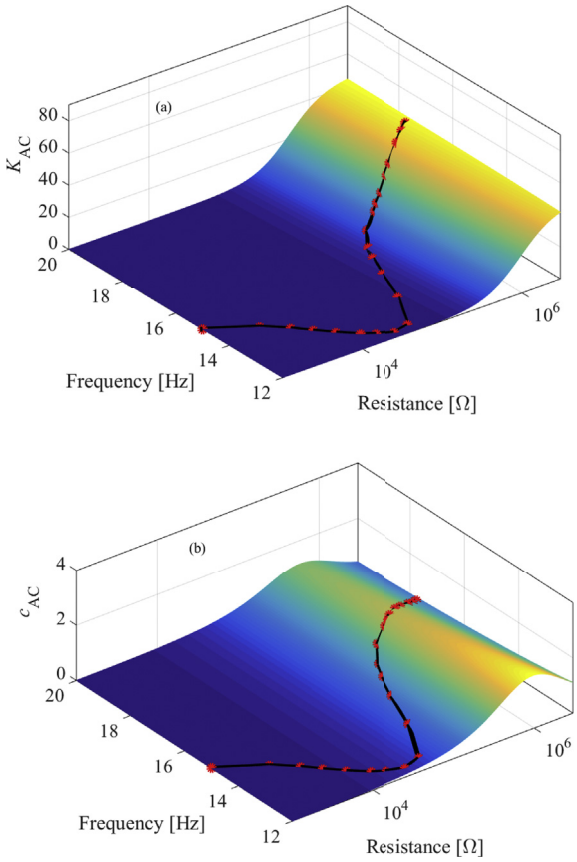

Fig. 6. (a) Equivalent stiffness K_{AC} and (b) equivalent damping c_{AC} induced by strong electromechanical coupling ($\Theta = 2000\ \mu N/V$, $A_0 = 2.0\ ms^{-2}$).

To summarize the above discussion, two optimal power peaks are obtained in the strong electromechanical coupling condition, contrasting the only one power peak in the weak coupling condition. One is close to the short circuit, and the other close to the open circuit. As compared to the linear PEH, the monostable PEH has much complex characteristics of resonant peak shift and operation bandwidth variance. For the monostable PEH, the high-energy large-amplitude oscillation is more sensitive to the equivalent damping than stiffness when the resistance is very small. The equivalent damping induced by AC interface circuit will remarkably shrink the range of the useful bandwidth (peak shifts to the left). The continuous increase of the resistance will then enable the equivalent stiffness to dominate the shift of the resonant peak, which is similar to the behaviour of linear energy harvester. All the results of theory and ECM simulation are very consistent both qualitatively and quantitatively.

3.2. DC interface

In this section, the effects of DC interface circuit on the performance of monostable PEH are investigated and compared with that of AC interface circuit in terms of resistance, acceleration and electromechanical coupling coefficient to identify the similarities and differences between these two interfaces.

3.2.1. Effect of load resistance

Fig. 7 depicts the output power of the monostable PEH with varying resistance R_L in the DC interface circuit. As aforementioned, for the DC interface circuit, stability is inherent to the output since an analytically derived Jacobian is provided to the algorithm. The results only consequently converge to stable responses. First, both theoretical prediction and ECM simulation (upward sweep) result indicate that, the DC power outputs (computed according to V^2/R_L) are reduced but with a higher optimal resistance $R_L = 200\ k\Omega$, compared to the results with AC interface circuit (Fig. 2). Second, the resonant peak shifts to the left and then returns to the right with the increase of R_L, with the turning point close to $R_L = 200\ k\Omega$. These observations are similar to those of AC interface circuit. In addition, though the shift of the resonant peak with the DC interface circuit is less than that with the AC interface circuit, it is still more noticeable than the linear PEH. Moreover, the small discrepancy between theory and ECM simulations is the ripples in the DC voltage in the ECM simulation rather than ideal steady-state results. The ripples can be reduced in simulation by using a large C_f. However, C_f cannot be too large since we would like the harvester to reach quasi-steady-state very quickly, which is dependent on the time constant $C_f R_L$. While in

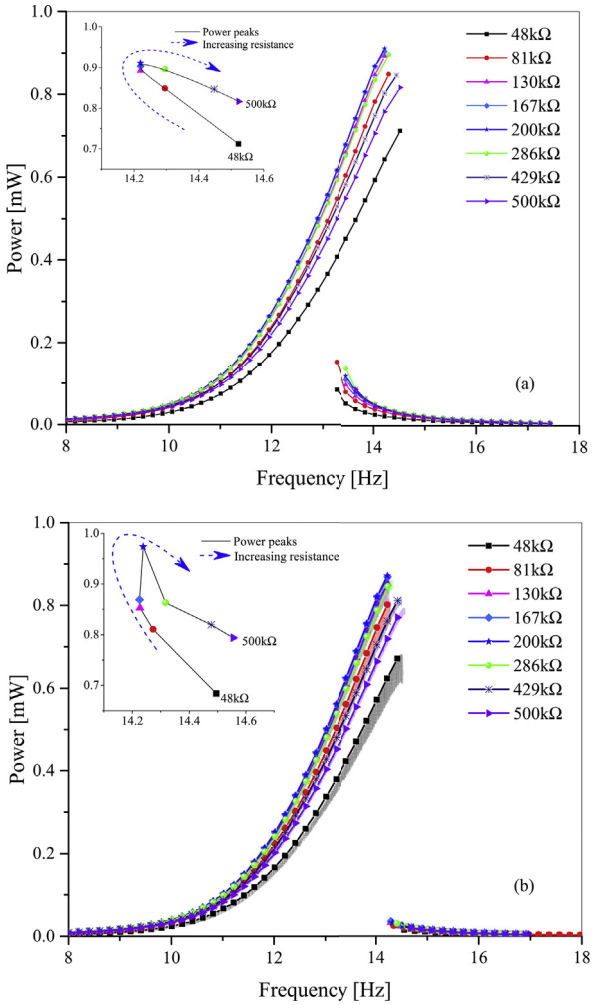

Fig. 7. Output powers of theory and ECM with DC interface circuit for weak electromechanical coupling ($\Theta = 599\ \mu N/V$, $A_0 = 2.0\ ms^{-2}$). (a) theory; (b) ECM [25].

the approximate solutions based on the harmonic balance analysis, no ripple is expected as we assume harmonic solution in the steady state with a correspondingly large C_f. Fortunately, despite the existence of ripples in the ECM simulation, they do not affect the main features of the responses, such as peak shift and bandwidth. From Fig. 7, we conclude that for the monostable PEH with DC interface circuit, the trade-off is still required between maximizing the power and bandwidth, though the sacrifice of bandwidth is less than that in the case of AC interface circuit.

3.2.2. *Effect of excitation*

Fig. 8 presents the output power of the monostable PEH with the DC interface circuit under various accelerations: $A_0 = 1\ ms^{-2}$, $2\ ms^{-2}$, $3\ ms^{-2}$, $4\ ms^{-2}$. The resistance used here $R_L = 200\ k\Omega$ is the optimal resistance obtained from the previous section. Both the theoretical and ECM results show that the bandwidth and resonant peak will increase due to the increase of excitation. The characteristics of DC interface circuit are similar to that of AC interface circuit. First, when the acceleration increases, the high-energy large-amplitude oscillation is obtained in a much wider frequency bandwidth. Second, the output power of high-energy oscillation benefits very few from the increase of acceleration level. For instance, at $f = 15$ Hz, the output power with $A_0 = 3\ ms^{-2}$ are very close to that with $A_0 = 4\ ms^{-2}$. For a certain acceleration, the power output with DC interface circuit is much lower than that with AC interface circuit. For example, when $A_0 = 4\ ms^{-2}$, the generated power of DC interface circuit is 3.253 mW while that of AC interface circuit is 7.755 mW, that is, 58.05% less. Meanwhile, in terms of the region of coexisting responses, it is $\Delta f = 3.514$ HZ (from 14.288 HZ to 17.802 HZ) for the DC interface circuit, while it is $\Delta f = 2.7326$ HZ (from 14.418 HZ to 17.151 HZ) for the AC interface circuit. Consequently, for a certain resistance, the AC interface circuit may have a larger output power while the DC interface circuit maintains a wider bandwidth of high-energy oscillations. The decrease of output power when monostable PEH is connected to DC interface circuit is mainly due to the fact that energy transfer stops if the voltage V across the piezoelectric transducer is lower than the DC voltage V_f in a certain duration of one oscillation period, which is similar to the linear PEH case. Since it has been proven in Ref. [37] that the rectifying circuit can be treated by impendence

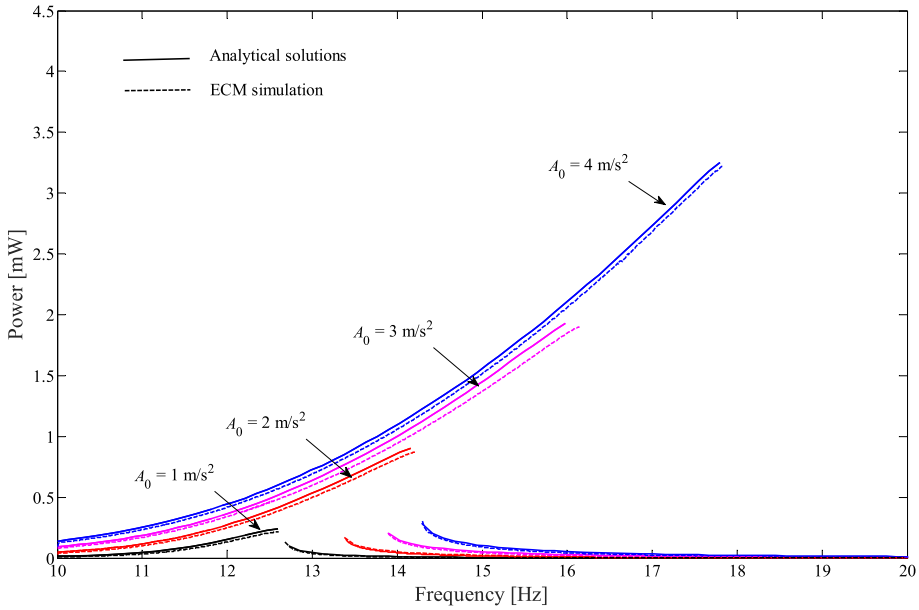

Fig. 8. Output powers of theory and ECM with DC interface circuit for different accelerations ($\Theta = 599\ \mu N/V$, $R_L = 200\ k\Omega$).

analysis, these differences between AC and DC interface circuits can be further explained by the effect of effective resistance on monostable PEH. When the resistance is larger than the optimal resistance, the increase of R_L will result in a decrease of output power and a wider bandwidth of high-energy oscillation. The less power extracted from DC interface circuit, in turn, induces less equivalent damping and gives rise to a larger vibrating response and more evident nonlinear behaviour (wider region of coexisting responses) as compared to AC interface circuit.

Though the analytical results agree quite well with the ECM simulations, discrepancy still exists. The main discrepancy is that the resonant peak of ECM simulation is a bit shifted as compared to that of analytical results. This discrepancy results from the assumption in theoretical analysis. In the theoretical analysis, we assume steady state periodic response when we derive the solution. However, in simulation, though we use a slow frequency sweep rate (0.02 Hz/s), the response is close to but still transient rather than exact steady state response. This will be a bit worse in DC interface circuit case because we have not only transients in dynamic response but also transients in electrical response. The electrical output takes time to reach steady state that depends on the time constant of the interface circuit (load resistor and filter capacitor). A small filter capacitor will ensure to reach quasi-steady state but end up with ripples in DC voltage (for example, Fig. 7(b)), while a large filter capacitor will remove ripples but take a longer time to reach steady state. This, combined with the transient in dynamics, makes the delay in jumping (a minor difference in resonant peak) in Fig. 8. In this work, we choose such a capacitor to compromise: relatively small ripples and minor delay in jumping.

3.2.3. *Effect of electromechanical coupling strength*

The electromechanical coupling coefficient is increased to $\Theta = 2000\ \mu N/V$ to explore the effect of strong coupling on the performance of the monostable PEH with DC interface circuit. Fig. 9 shows the output power with varying resistance R_L (listed in Table 3) from theoretical prediction and ECM simulation (upward sweep). Similarities between AC and DC interface circuits are noted in Fig. 9. First, when R_L increases from 1 kΩ to 10 kΩ, the bandwidth of high-energy large-amplitude oscillation decreases remarkably, accompanied with the increase of peak power and shift to the lower frequency. Second, when R_L increases from 15 kΩ to 130 kΩ, the resonant peak decreases gradually and the region of coexisting responses and jumping phenomenon disappear. Subsequently, when R_L further increase to 2500 kΩ, the resonant peak reaches second peak at $R_L = 2000$ kΩ. Similar to the AC interface circuit, when R_L is 2500 kΩ, the jump phenomenon returns in the theoretical results. Another similarity between the effect of AC and DC interface circuits is that the first peak ($R_L = 10$ kΩ) is close to short circuit, while the second peak ($R_L = 2000$ kΩ) is close to open circuit. The main difference by using these two different interface circuits is the output power. By comparing Figs. 5 and 9, it is noted that the maximum output power of AC circuit is 2.19 mW while that of DC circuit is about 1.09 mW.

4. Experimental validation

Experiments are conducted to confirm the conclusions in section 3. Since the coupling strength could not be altered after prototyping the device, experiment is not ready to confirm the effect of strong electromechanical coupling. The nonlinear

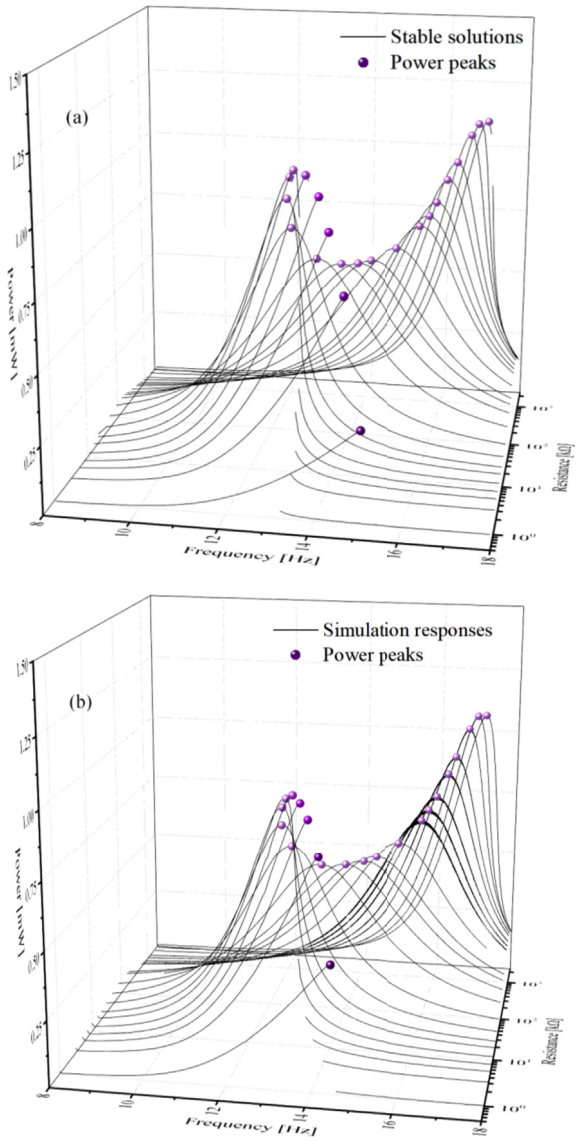

Fig. 9. Output powers of theory and ECM with DC interface circuit for strong electromechanical coupling ($\Theta = 2000\,\mu N/V$, $A_0 = 2.0\,ms^{-2}$). (a) theory; (b) ECM.

energy harvester is prototyped using a bimorph piezoelectric transducer (MIDE Technologies, model: V21BL). Two cylindrical permanent magnets are used as the repulsive magnet pair; the magnets have thickness 3 mm and diameter 8 mm. The base excitation is generated by an electrodynamic shaker (APS Dynamics, model: APS 113) electronically governed in a feedback-based vibration controller (Vibration Research, model: VR9500). The output voltages and currents across and through the

Table 3
Power peaks with strong electromechanical coupling for various resistances of DC interface.

Resistance (kΩ)	1	3	5	7	10	15	20	30
Peak Freq. (Hz)	15.03	14.44	13.99	13.69	13.32	12.95	12.80	12.65
Power (mW)	0.333	0.728	0.924	1.029	1.087	1.086	1.048	0.952
Resistance (kΩ)	48	81	130	167	200	286	429	500
Peak Freq. (Hz)	12.66	13.17	13.69	14.07	14.36	14.96	15.48	15.70
Power (mW)	0.825	0.688	0.649	0.642	0.646	0.678	0.749	0.783
Resistance (kΩ)	600	800	1000	1500	2000	2500		
Peak Freq. (Hz)	15.85	16.07	16.30	16.59	16.74	16.97		
Power (mW)	0.829	0.906	0.966	1.058	1.092	1.092		

load resistance are acquired by NI 9229 and NI 9203 DAQ modules. The details of parameter identification can be found in Ref. [25]. With these parameters and considering the electrical-mechanical equivalence, circuit simulation parameters are identified.

4.1. AC interface

4.1.1. Effect of load resistance

The power output against varying resistive loads *R*L with AC interface circuit is shown in Fig. 10. These results are adopted from Ref. [25] for comparison with theoretical analysis as well as ECM simulation. Slow upward sweeps are performed with the same excitation as theoretical analysis. Though the magnitude of power estimated from theory and ECM simulation is a bit higher than that in the experiment, the trend is the same: the power peak first shifts to the left when R_L increases from 48 kΩ and reaches the maximum at $R_L = 167$ kΩ. With the further increase of R_L, the power peak turns to the high frequency with a loss in power output. The experimental results confirm the theoretical and ECM observation that given the same electromechanical coupling, the varying resistance of AC interface circuit has much more significant influence on the dynamics of the monostable PEH than that on the linear PEH in terms of resonant peak shift and thus the associated bandwidth.

4.1.2. Effect of excitation

Fig. 11 indicates the upward sweep responses of the monostable PEH with varying accelerations when connected with AC interface circuit. The accelerations chosen are 1 ms^{-2}, 2 ms^{-2}, 3 ms^{-2} and 4 ms^{-2}, same as those in theoretical analysis and ECM simulation. It is noted that the operational bandwidth of the monostable PEH largely increases with the increase of excitation. The jumping frequencies in these sweeps are 10.2 Hz, 13.05 Hz, 15.2 Hz and 16.9 Hz respectively, which is close to

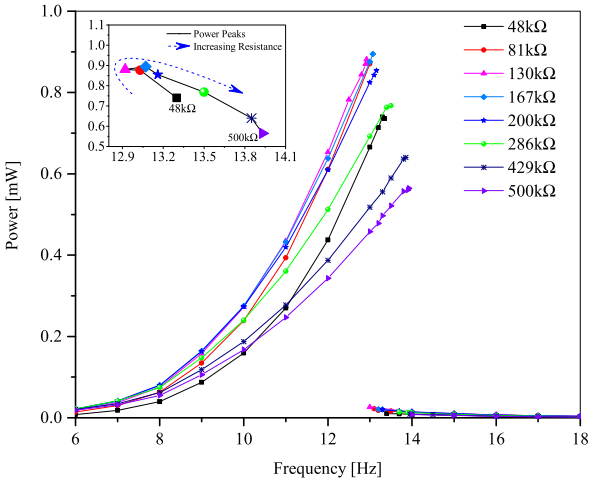

Fig. 10. Output powers of experiment with AC interface circuit for weak electromechanical coupling coefficient ($\Theta = 599$ μN/V, $A_0 = 2.0$ ms^{-2}) [25].

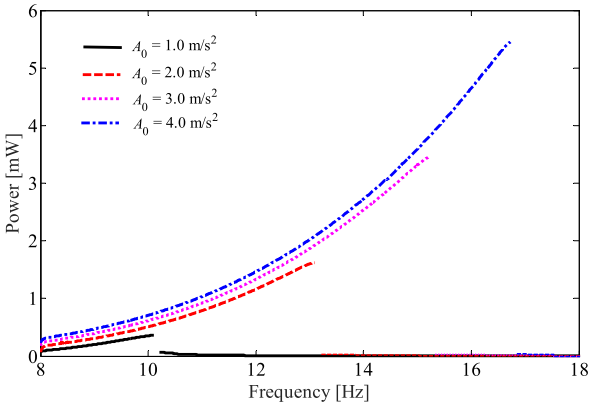

Fig. 11. Output powers of experiment with AC interface circuit for different accelerations ($\Theta = 599$ μN/V, $R_L = 167$ kΩ).

the theory and ECM simulations. Meanwhile, by comparing the output power of the high-energy oscillations under different excitations, it is found that the increase of excitation gives minor improvement in output power, while it does enlarge the bandwidth dramatically. The main characteristics in the experiment quantitatively agree with the simulation and theoretical analysis, though discrepancies still exist. For instance, under low excitation of $A_0 = 1\ \mathrm{ms}^{-2}$, the experimental response shows the jumping phenomenon, which is not found in the simulation.

4.2. DC interface

4.2.1. Effect of load resistance

The performance of the monostable PEH connected to DC interface circuit with varying resistance is shown in Fig. 12. These upward sweep results are adopted from Ref. [25] for comparison with theoretical analysis as well as ECM simulation. First, the DC power outputs are reduced but with a higher optimal resistance 200 kΩ, compared to the results with AC interface circuit (Fig. 10), similar to those of linear PEH with AC and DC interface circuits [26]. The difference in power level is due to the fact that the rectifying DC circuit does not extract energy all the time during one vibrational period, which is similar to the linear PEH. Second, the increasing resistance results in a decrease of bandwidth and an improvement of output power until it reaches the maximum power. The bandwidth increases with a sacrifice of output power beyond the maximum power point. Meanwhile, a similar trend in peak shift and operational bandwidth is observed by contrasting AC and DC interface circuits. All these features confirm what we observed in theoretical analysis and ECM simulation.

4.2.2. Effect of excitation

The effect of excitation when connected to DC interface circuit is shown in Fig. 13. Four different acceleration levels chosen are the same as those in Section 4.1.2. With the increase of excitation, the bandwidth is largely broadened. The jumping frequencies during upward sweeps are 9.8 Hz, 13.0 Hz, 15.2 Hz and 16.9 Hz for different accelerations. Effects of AC and DC interface circuits on the monostable PEH in the experiment are similar to those observed in theoretical analysis and ECM simulation. The bandwidth is largely enhanced by shifting the resonant peak with the increase of excitation but the output power increases very little at a certain frequency. Moreover, the AC interface circuit can produce more power than the DC interface circuit for various excitation by contrasting Figs. 11 and 13.

5. Conclusions

In this paper, the performances of AC and DC interface circuits on monostable piezoelectric energy harvesters are analyzed and compared based on harmonic balance analysis, equivalent circuit modeling and experiment. The effects of three critical factors — load resistance, electromechanical coupling and excitation levels are investigated and compared when monostable PEH is connected to AC and DC interface circuits.

Several conclusions have been drawn after a comprehensive parametric study: **(1)** The effect of AC interface circuit on monostable PEH can be regarded as an equivalent damping and stiffness, which are determined by the frequency of excitation, resistance, capacitance and electromechanical coupling. The effect of circuit-induced damping is more dominant than that of circuit-induced stiffness when the load resistance is low, which results in the power peak shift to a lower frequency with a narrow bandwidth. As the load resistance becomes large enough, the increase of resistance will lead to the power peak

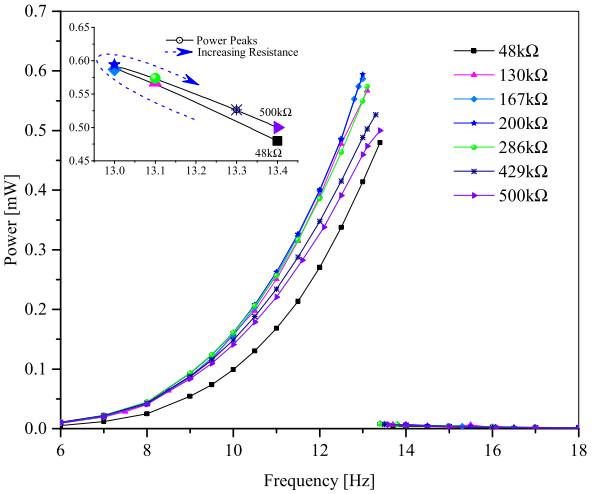

Fig. 12. Output powers of experiment with DC interface circuit for weak electromechanical coupling coefficient ($\Theta = 599\ \mu\mathrm{N/V}$, $A_0 = 2.0\ \mathrm{ms}^{-2}$) [25].

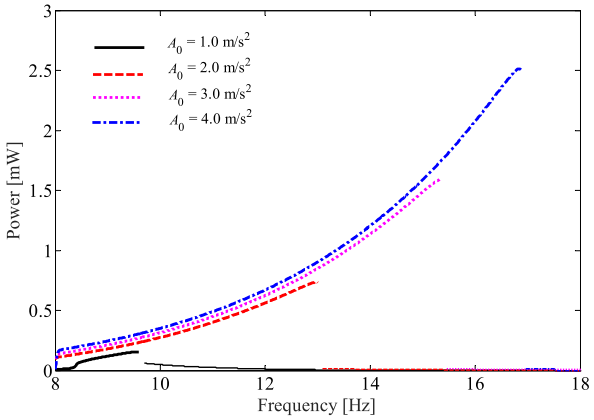

Fig. 13. Output powers of experiment with DC interface circuit for different accelerations ($\Theta = 599$ μN/V, $R_L = 200$ kΩ).

shift to a higher frequency but a lower harvested power; **(2)** Similarity and difference are observed by comparing the effects of interface circuits on the performances of the monostable and linear PEHs given different electromechanical couplings. The similarity is that for the weak electromechanical coupling, only one optimal power peak exits for both monostable and linear PEHs, while two optimal power peaks are observed for the strong coupling, with one peak being close to the short circuit and the other close to the open circuit. The difference is that the power peak shift of the monostable PEH with either AC or DC interfaces follows a unique routine as load resistance increases and therefore the interface circuits show more significant impact on the nonlinear PEH than that on the linear PEH in terms of bandwidth; **(3)** Comparing the characteristics with AC and DC interface circuits in terms of peak shift and the consequent bandwidth change, The trends are very similar for three parameters concerned: varying load resistance, excitation, and electromechanical coupling. The main difference between AC and DC interface circuits is that AC interface circuit achieves a higher maximum power with a relatively lower optimal load resistance as compared to DC interface circuit. Meanwhile, the power peak shift with AC interface is more evident than that with DC interface.

Acknowledgement

Chunbo Lan acknowledges the financial support from the China Scholarship Council (Grant No. 201506290096), National Natural Science Foundation of China (Grant No. 11172234), Innovation Foundation for Doctor Dissertation of Northwestern Polytechnical University (No. CX201614) and Excellent Doctorate Foundation of Northwestern Polytechnical University (W099108). Ryan L Harne acknowledges the support from the Center for Automotive Research at The Ohio State University.

Appendix

The governing equations of monostable PEH are,

$$\left\{ M_{\text{eff}}\ddot{x} + C_{\text{eff}}\dot{x} + k_0 x - \Theta v + K_3 x^3 = f\cos(\omega t) v/R_L + C_p\dot{v} + \Theta\dot{x} = 0 \right. \tag{A.1}$$

where $k_0 = K_{\text{eff}} + K_1$; $f = M_{\text{eff}}A_0$.

Assume the appropriate solutions have the following form,

$$\left\{ \begin{array}{l} x = a_1\sin(\omega t) + b_1\cos(\omega t) \\ v = a_2\sin(\omega t) + b_2\cos(\omega t) \\ \dot{x} = a_1\omega\cos(\omega t) - b_1\omega\sin(\omega t) \\ \dot{v} = a_2\omega\cos(\omega t) - b_2\omega\sin(\omega t) \\ \ddot{x} = -a_1\omega^2\sin(\omega t) - b_1\omega^2\cos(\omega t) \end{array} \right. \tag{A.2}$$

Substituting Eq. (A.2) into the first expression of Eq. (A.1), neglecting the higher harmonics and balancing the terms of $\sin(\omega t)$ and $\cos(\omega t)$, we obtain

$$a_1\left(-\omega^2 M_{\text{eff}} + k_0 + \frac{3}{4}r^2 K_3 \right) - b_1\omega C_{\text{eff}} - \Theta a_2 = 0 \tag{A.3}$$

$$b_1\left(-\omega^2 M_{\text{eff}}+k_0+\frac{3}{4}r^2K_3\right)+C_{\text{eff}}a_1\omega-\Theta b_2=f \tag{A.4}$$

where $r^2=\mathrm{b}_1^2+\mathrm{a}_1^2$.

Applying the same procedure into the second expression of Eq. (A.1) yields

$$a_2/R_{\text{L}}-C_{\text{p}}b_2\omega-b_1\omega\Theta=0 \tag{A.5}$$

$$b_2/R_{\text{L}}+C_{\text{p}}a_2\omega+\Theta a_1\omega=0 \tag{A.6}$$

Since Eqs. (A.5) and (A.6) are linear, the electrical coefficients a_2 and b_2 can be solved as

$$\begin{cases} a_2=\dfrac{-\Theta C_{\text{p}}(R_{\text{L}}\omega)^2a_1+\Theta R_{\text{L}}\omega b_1}{\left(C_{\text{p}}R_{\text{L}}\omega\right)^2+1} \\ b_2=\dfrac{-\Theta R_{\text{L}}\omega a_1-(R_{\text{L}}\omega)^2C_{\text{p}}\Theta b_1}{\left(C_{\text{p}}R_{\text{L}}\omega\right)^2+1} \end{cases} \tag{A.7}$$

Substituting the steady-state solutions for a_2 and b_2 into Eqs. (A.3) and (A.4), we obtained the expression of frequency-amplitude of monostable PEH shown as follows,

$$r^2\left[\left(-\omega^2M_{\text{eff}}+k_0+\frac{3}{4}r^2K_3+\frac{C_{\text{p}}(\Theta R_{\text{L}}\omega)^2}{\left(C_{\text{p}}R_{\text{L}}\omega\right)^2+1}\right)^2+\left(\omega C_{\text{eff}}+\frac{\Theta^2R_{\text{L}}\omega}{\left(C_{\text{p}}R_{\text{L}}\omega\right)^2+1}\right)^2\right]=f^2 \tag{A.8}$$

More interestingly, by substituting Eq. (A.7) into the second expression of Eq. (A.2), we obtain

$$v=\frac{-\Theta C_{\text{p}}(R_{\text{L}}\omega)^2a_1+\Theta R_{\text{L}}\omega b_1}{\left(C_{\text{p}}R_{\text{L}}\omega\right)^2+1}\sin(\omega t)+\frac{-\Theta R_{\text{L}}\omega a_1-(R_{\text{L}}\omega)^2C_{\text{p}}\Theta b_1}{\left(C_{\text{p}}R_{\text{L}}\omega\right)^2+1}\cos(\omega t) \tag{A.9}$$

Rearranging Eq. (A.9) yields

$$v=-\frac{(R_{\text{L}}\omega)^2C_{\text{p}}\Theta}{\left(C_{\text{p}}R_{\text{L}}\omega\right)^2+1}(a_1\sin(\omega t)+b_1\cos(\omega t))-\frac{\Theta R_{\text{L}}}{\left(C_{\text{p}}R_{\text{L}}\omega\right)^2+1}(\omega a_1\cos(\omega t)-\omega b_1\sin(\omega t)) \tag{A.10}$$

Substituting the first and third expression of Eq. (A.2) into Eq. (A.10) and eliminating a_1 and b_1, we obtain

$$v=-\frac{(R_{\text{L}}\omega)^2C_{\text{p}}\Theta}{\left(C_{\text{p}}R_{\text{L}}\omega\right)^2+1}x-\frac{\Theta R_{\text{L}}}{\left(C_{\text{p}}R_{\text{L}}\omega\right)^2+1}\dot{x} \tag{A.11}$$

Thus, the electromechanical coupling force in Eq. (A.1) can be expressed as

$$-\Theta v=\frac{(R_{\text{L}}\omega\Theta)^2C_{\text{p}}}{\left(C_{\text{p}}R_{\text{L}}\omega\right)^2+1}x+\frac{\Theta^2R_{\text{L}}}{\left(C_{\text{p}}R_{\text{L}}\omega\right)^2+1}\dot{x} \tag{A.12}$$

Finally, based on Eq. (A.12), we find that the effect of AC interface circuit on the monostable PEH is to change its stiffness and damping. The equivalent stiffness and damping caused by the circuit through electromechanical coupling are

$$K_{\text{AC}}=\frac{(R_{\text{L}}\omega\Theta)^2C_{\text{p}}}{\left(C_{\text{p}}R_{\text{L}}\omega\right)^2+1},c_{\text{AC}}=\frac{\Theta^2R_{\text{L}}}{\left(C_{\text{p}}R_{\text{L}}\omega\right)^2+1} \tag{A.13}$$

From Eq. (A.13), we find that the equivalent stiffness K_{AC} and equivalent damping c_{AC} induced by the circuit depend on the external excitation frequency ω, the load resistance R_{L}, the capacitance of the piezoelectric element C_{p}, and the electromechanical coupling Θ.

References

[1] M.F. Daqaq, R. Masana, A. Erturk, D.D. Quinn, On the role of nonlinearities in vibratory energy harvesting: a critical review and discussion, Appl. Mech. Rev. 66 (2014), 040801.
[2] R. Harne, K. Wang, A review of the recent research on vibration energy harvesting via bistable systems, Smart Mater. Struct. 22 (2013), 023001.
[3] C. Wei, X. Jing, A comprehensive review on vibration energy harvesting: modelling and realization, Renew. Sustain. Energy Rev. 74 (2017) 1–18.
[4] H. Wu, L. Tang, Y. Yang, C.K. Soh, A novel 2-DOF piezoelectric energy harvester, in: 22nd International Conference on Adaptive Structures and Technologies (ICAST), Corfu, Greece, 2011, p. 077.
[5] S.C. Stanton, C.C. McGehee, B.P. Mann, Nonlinear dynamics for broadband energy harvesting: investigation of a bistable piezoelectric inertial generator, Physica D 239 (2010) 640–653.
[6] S.C. Stanton, C.C. McGehee, B.P. Mann, Reversible hysteresis for broadband magnetopiezoelastic energy harvesting, Appl. Phys. Lett. 95 (2009), 174103.
[7] B. Mann, N. Sims, Energy harvesting from the nonlinear oscillations of magnetic levitation, J. Sound Vib. 319 (2009) 515–530.
[8] A. Erturk, J. Hoffmann, D. Inman, A piezomagnetoelastic structure for broadband vibration energy harvesting, Appl. Phys. Lett. 94 (2009), 254102.
[9] A. Erturk, D. Inman, Broadband piezoelectric power generation on high-energy orbits of the bistable Duffing oscillator with electromechanical coupling, J. Sound Vib. 330 (2011) 2339–2353.
[10] H. Wu, L. Tang, Y. Yang, C.K. Soh, Development of a broadband nonlinear two-degree-of-freedom piezoelectric energy harvester, J. Intell. Mater. Syst. Struct. 25 (2014) 1875–1889.
[11] S. Zhou, J. Cao, W. Wang, S. Liu, J. Lin, Modeling and experimental verification of doubly nonlinear magnet-coupled piezoelectric energy harvesting from ambient vibration, Smart Mater. Struct. 24 (2015), 055008.
[12] W.J. Su, J. Zu, Y. Zhu, Design and development of a broadband magnet-induced dual-cantilever piezoelectric energy harvester, J. Intell. Mater. Syst. Struct. 25 (2014) 430–442.
[13] L. Xiong, L. Tang, H. Ding, L. Chen, B. Mace, Broadband performance of a piezoelectric energy harvester based on the internal resonance of buckled beam, in: Proc. SPIE, 2016, pp. 97993O-97993O-97911.
[14] L. Xiong, L. Tang, B.R. Mace, Internal resonance with commensurability induced by an auxiliary oscillator for broadband energy harvesting, Appl. Phys. Lett. 108 (2016), 203901.
[15] L.Q. Chen, G.C. Zhang, H. Ding, Internal resonance in forced vibration of coupled cantilevers subjected to magnetic interaction, J. Sound Vib. 354 (2015) 196–218.
[16] C. Lan, W. Qin, W. Deng, Energy harvesting by dynamic unstability and internal resonance for piezoelectric beam, Appl. Phys. Lett. 107 (2015), 093902.
[17] L.Q. Chen, W.-A. Jiang, Internal resonance energy harvesting, J. Appl. Mech-T. ASME 82 (2015), 031004.
[18] N. Kong, D.S. Ha, A. Erturk, D.J. Inman, Resistive impedance matching circuit for piezoelectric energy harvesting, J. Intell. Mater. Syst. Struct. 21 (2010) 1293–1302.
[19] D. Guyomar, A. Badel, E. Lefeuvre, C. Richard, Toward energy harvesting using active materials and conversion improvement by nonlinear processing, IEEE Trnas. Ultrason Ferr. 52 (2005) 584–595.
[20] J. Liang, W.-H. Liao, Improved design and analysis of self-powered synchronized switch interface circuit for piezoelectric energy harvesting systems, IEEE Trans. Ind. Electron. 59 (2012) 1950–1960.
[21] Y. Shu, I. Lien, Analysis of power output for piezoelectric energy harvesting systems, Smart Mater. Struct. 15 (2006) 1499.
[22] A. Erturk, D.J. Inman, Piezoelectric Energy Harvesting, John Wiley & Sons, 2011.
[23] C.J. Rupp, M.L. Dunn, K. Maute, Analysis of piezoelectric energy harvesting systems with non-linear circuits using the harmonic balance method, J. Intell. Mater. Syst. Struct. 21 (2010) 1383–1396.
[24] W.Q. Liu, A. Badel, F. Formosa, Y.P. Wu, A. Agbossou, Wideband energy harvesting using a combination of an optimized synchronous electric charge extraction circuit and a bistable harvester, Smart Mater. Struct. 22 (2013), 125038.
[25] L. Tang, Y. Han, J. Hand, R.L. Harne, Exploring the roles of standard rectifying circuits on the performance of a nonlinear piezoelectric energy harvester, in: Proc. SPIE, 2016, p. 9799.
[26] A. Erturk, D.J. Inman, On mechanical modeling of cantilevered piezoelectric vibration energy harvesters, J. Intell. Mater. Syst. Struct. 19 (2008) 1311–1325.
[27] F. Cottone, H. Vocca, L. Gammaitoni, Nonlinear energy harvesting, Phys. Rev. Lett. 102 (2009), 080601.
[28] S. Leadenham, Advanced Concepts in Nonlinear Piezoelectric Energy Harvesting: Intentionally Designed, Inherently Present, and Circuit Non-linearities, Georgia Institute of Technology, 2015.
[29] S.C. Stanton, B.A. Owens, B.P. Mann, Harmonic balance analysis of the bistable piezoelectric inertial generator, J. Sound Vib. 331 (2012) 3617–3627.
[30] M.A. Karami, D.J. Inman, Equivalent damping and frequency change for linear and nonlinear hybrid vibrational energy harvesting systems, J. Sound Vib. 330 (2011) 5583–5597.
[31] Z. Wu, R.L. Harne, K.-W. Wang, Energy harvester synthesis via coupled linear-bistable system with multistable dynamics, J. Appl. Mech-T. ASME 81 (2014), 061005.
[32] S. Zhou, J. Cao, D.J. Inman, J. Lin, D. Li, Harmonic balance analysis of nonlinear tristable energy harvesters for performance enhancement, J. Sound Vib. 373 (2016) 223–235.
[33] K.S. Kundert, A. Sangiovanni-Vincentelli, Simulation of nonlinear circuits in the frequency domain, IEEE Trans. Comput. AID. D. 5 (1986) 521–535.
[34] R. Harne, K. Wang, On the fundamental and superharmonic effects in bistable energy harvesting, J. Intell. Mater. Syst. Struct. 25 (2014) 937–950.
[35] L. Zhao, L. Tang, Y. Yang, Synchronized charge extraction in galloping piezoelectric energy harvesting, J. Intell. Mater. Syst. Struct. 27 (2016) 453–468.
[36] L. Zhao, L. Tang, J. Liang, Y. Yang, Synergy of wind energy harvesting and synchronized switch harvesting interface circuit, IEEE/ASME Trans. Mech 22 (2017) 1093–1103.
[37] J. Liang, W.H. Liao, Impedance modeling and analysis for piezoelectric energy harvesting systems, IEEE/ASME Trans. Mech. 17 (2012) 1145–1157.